https://doi.org/10.48048/tis.2024.7508

Coastal Evolution of Satingpra Peninsula, Songkhla Province: Implications for Understanding Songkla Lagoon Formation

Araf Laerosa[1,2], Siriporn Pradit[1,2], Komrit Wattanavatee[3], Helmut Duerrast[3], Tidarat Vichaidid[4], Montri Luengchavanon[1] and Prakrit Noppradit[1,2,*]

[1]Faculty Environmental Management, Princes of Songkla University, Songkhla 90110, Thailand
[2]Coastal Oceanography and Climate Change Research Center, Princes of Songkla University, Songkhla 90110, Thailand
[3]Division of Physical Science, Faculty of Science, Princes of Songkla University, Songkhla 90110, Thailand
[4]Department of Science, Faculty of Science and Technology, Prince of Songkla University, Pattani 94000, Thailand

([*]Corresponding author's e-mail: prakrit.n@psu.ac.th)

Received: 18 September 2023, Revised: 31 October 2023, Accepted: 7 December 2023, Published: 10 April 2024

Abstract

Songkhla Lagoon has been studied for decades, but there is no clear evidence of its origin. As a barrier to the lagoon, the Satingpra Peninsula plays a crucial role in understanding its formation. Eleven sediment samples from sand ridges and tidal flats on the Satingpra Peninsular were collected and analysed for granulometry and geochronology. Both coarse-grained and fine-grained quartz-rich fractions were utilised to prepare samples of aliquots. The optically stimulated luminescence (OSL) dating was performed using the single-aliquot regenerative dose method for a determined (deposited) age. In addition, previous research, geological surveys and geochronological data were combined to explain their formation in this region. The OSL ages in the present study indicated that the late Holocene regression occurred between 0.36 and 3.27 ka (ka stands for 1,000 years). Integrated with previous studies, recorded ages dating back to the mid-Holocene sea level rise (ca. 6.5 ka) and the subsequent late-Holocene decline, indicate that both the old lagoon and middle beach ridge exhibit a sand ridge formation that runs parallel to the shoreline, extending from the south to the north. The middle sand, in this study, formed from about 3.02 to 1.5 ka ago resulting in the lagoon being isolated from the sea during that time. The lagoonal tide led the deposition as the present tidal flat from 3.3 to 1.7 ka. About 2.19 ka ago, the inner and middle ridges formed due to wind-driven processes influenced by a dry climate. This was followed by a continued sea level regression, leading to the formation of the outer ridge around 1.5 ka ago when the sea level was 1.4 m below the present sea level. However, it's essential to consider this sea level data in relation to the tectonic and human-induced land motions in the surrounding area.

Keywords: Beach ridge, Coastal evolution, OSL dating, Sathingpra peninsula, Songkhla lagoon

Introduction

Beach ridges are prominent landforms that develop along coastlines worldwide, characterized by parallel ridges and swales adjacent to the shoreline. Barrier islands, spits and strain plains all contribute to the formation of beach ridges as part of the beach ridge system. Primarily, beach ridges are formed by a combination of numerous factors, such as wave-driven action, longshore drift, aeolian processes [1-3], human activity [3] and fluctuations in sea level over time [2-4]. A sequence of beach ridges and swales behind the ridges can provide a relative chronological geological and environmental record [2]. Sediments in beach ridges can be characterized by wave built-facies, which are usually covered by sand accretion due to wind activity [2,5]. The sediment itself can hold records of past coastal processes, environmental conditions, climate, the direction of the longshore current, as well as wind direction and speed, and even natural hazards such as storms [6] and tsunamis [7,8]. In addition to serving as an indicator of shore position and form, they can also be used to indirectly measure changes in sea level [5].

Beach ridges, as significant coastal geomorphological features, are also important for the study of paleoenvironments and paleoclimates, in particular, paleo sea level. To comprehend past sea levels, identifying and quantifying sea level indicators within stratigraphic sections of beach ridge sequences is frequently necessary. These indicators, as well as markers, are observed in shore regions where land and

ocean interact; mainly, the transition between shoreface (SF) and foreshore (FS), foreshore (FS) and backshore (BS) [5], or aeolian deposits, and particularly markers of storm wave swash height (SWSH) and ordinary berm (ob) [9]. Furthermore, these markers must also be considered along with other characteristics of sediment, such as grain size, sorting and colour.

Numerous studies in Thailand have successfully investigated coastal evolution and sea level changes in the past using different dating techniques such as radiocarbon dating (^{14}C) [10], thermoluminescence (TL) [11] and optically stimulated luminescence (OSL) dating [1,10,12], with the ^{14}C dating technique widely accepted in the study of the environment during the Quaternary period. This technique, however, required specific materials such as marine fossils or peat, which are rarely preserved on sandy beaches. Hence, OSL dating method has become prevalent in the determination of chronological sequences in sandy formations, encompassing beach ridges and loess deposits as such material is considered not to have been extensively reworked or contaminated by modern roots [13]. Further, the landforms reflect the abundance of feldspar and quartz grains, the 2 most important minerals used for age determination using OSL dating technique [1,14], and this method is more effective as it provides direct dating of sediment grains. Most effective OSL dating is a single aliquot regenerative dose method [15] called SAR protocol. Depending on the differences in the sediment properties, several techniques can be applied to improve the statistical value of the SAR, the central dose model (CDM) was introduced in 1999 [16]. Recently, the average dose model (ADM) was developed to reduce measurement uncertainty [17], however, the CDM usually applied.

The Sathingpra Peninsula was formed by the deposition of marine sediments during the last Holocene Sea level regression. Ridges exhibit alternating ridges and swales, characterized by the narrow and elongated complexity of sandy ridges located approximately 3 - 4 km away from the present-day coastline. They consist of 3 main ridges and several subsidiary ridges [18,19]. Among these, the central ridge is the largest. Sathingpra Peninsula encompases 4 districts in Songkhla province, including Ranot, Sathingpra, Krasae-sin and Singhanakhon, covering an area of approximately 800 km^2. It extends approximately 70 km from north to south and 5 - 13 km from east to west. The western side of the peninsular is the plain area of the Songkhla lagoon, characterized by a low-lying coastal area with an elevation of + 0.5 m above mean sea level (amsl). While on the eastern side, it borders the Gulf of Thailand and consists of sand ridges in a north-south direction, slightly higher in elevation compared to the western area. These ridges have an elevation of 1 - 2 m amsl. The sandy ridges provide settlement areas for the local communities, while the swales between the ridges serve as agricultural areas.

The study of chronological events on the beach ridges of the Sathigpra peninsula is still limited. Most research has focused on the surrounding area of Songkhla Lagoon, with only a few studies specifically targeting the beach ridges on the Sathingpra peninsula. Prior studies have primarily focused on economic geology, such as land allocation and exploration of mineral and construction material resources [20,21]. Previous studies on the beach ridges of the Sathingpra peninsula have investigated sediment deposition rates, sea-level changes and age estimation using ^{14}C dating and TL techniques [11,22-24]. Nevertheless, age determination has predominately been conducted on the prominent beach ridges in the southern part of the peninsula [24]. Furthermore, the ^{14}C age reported in previous studies was documented using the year before present (year BP). In order to enhance the accuracy and precision of ^{14}C dating, it is important to calibrate the ^{14}C ages from year BP to cal. BP due to the variation over time in the production of radiocarbon in the atmosphere. As a result, there is still insufficient data to completely comprehend the chronological events and environmental changes that occurred on the beach ridges of the Sathingpra peninsula during the late Quaternary period.

The purpose of this study is to develop a more robust geochronological framework for the Sathingpra Peninsula. Here, sediment deposited on 3 former beach ridges and the plains behind the ridges have been investigated. The sedimentological regime and stratigraphy of the beach ridge system in Sathingpra Peninsula are suitable for enhancing understanding of coastal processes, sea level fluctuations, environmental conditions and a time series of coastal evolution on Sathingpra Peninsula during the late Holocene by using quartz-OSL dating.

Materials and methods

Sampling sites and sample collection

The topographic map was generated with the 30 m-SRTM datasets acquired from NASA services [25], while geological maps [18,19] were employed to indicate the sampling site and landform. The geographic coordinates and surface altitudes of each OSL sampling location were measured in July 2022 using the Topcon hyper SR system and a real-time kinematic (RTK) survey. This survey was conducted utilising the network facilities provided by the Department of Land.

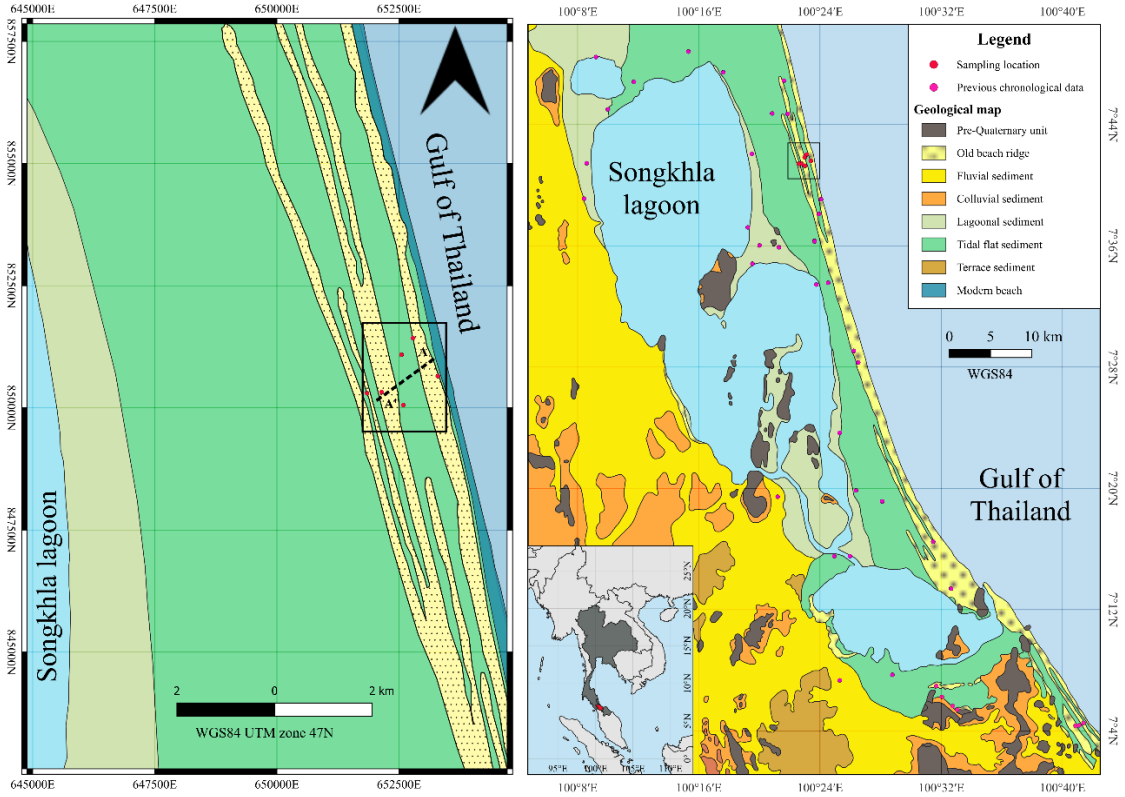

Figure 1 Sampling locations, red dots in box and previous geochronological data locations (pink dots) shown on modified geological map [18,19].

A total of 11 sediment samples were collected from distinct geological units [20,21], and as documented in geological maps [18,19]. In particular, 2 samples were obtained from the older beach ridge situated adjacent to the backshore area near to the present-day beach. Additionally, 2 more samples were acquired from a former beach ridge located farther away. The other 7 samples were collected from the older tidal flat. The sampling locations are shown in **Figure 1** as red dots.

The collection of samples involved the utilisation of a 3-inch-diameter opaque stainless-steel tube, which was horizontally inserted into specified regions of excavation pits and a trench through the application of hammering. To decrease the effect of soil development, bioturbation and human-caused processes, it was ensured that each sample was obtained at a minimum depth of 0.3 m below the surface [26]. The depths of the samples ranged from 0.35 - 2.00 m beneath the surface. Subsequently, the sample was immediately sealed at both ends to preserve its moisture content and shield it from any potential light exposure. Furthermore, in order to conduct grain size analysis, an additional 5 samples were obtained from the surrounding area of the OSL sampling site.

Sediment characterization

A group of 5 samples was obtained from 4 distinct pits and trenches for the objective of conducting grain size analysis. Samples were measured in terms of weight both before and after the process of drying. The samples were further analysed using mesh sizes of 38, 63, 125, 180, 250, 500, 1,000 and 2,000 µm. The weight of the sediment retained in each mesh was measured, and afterwards weight percentages were calculated. Geometric graphical measurements [27] were employed in MS Excel for calculating grain size statistics, including average grain size, sorting, skewness and kurtosis.

Table 1 Summary data of sampling sites including geographic coordinates, surface altitude, depth and aliquot preparation type (C: Coarse-grained fraction and F: Fine-grained fraction).

Sample ID	Latitude	Longitude	Altitude (m)	Depth (m)	Aliquot preparation
Rawa Beach					
SK01	7.693374603	100.38989	1.004	0.80	C
SK02	7.693374603	100.38989	1.004	1.33	C
Wat Pang tree					
SK03	7.700433252	100.38530	0.397	2.00	F
Palm garden					
SK04	7.697361856	100.38316	0.048	0.35	F
SK05	7.697361856	100.38316	0.048	1.12	F
SK06	7.697361856	100.38316	0.048	1.40	C
SK07	7.697361856	100.38316	0.048	1.60	F
Swale					
SK08	7.688037317	100.38348	0.26	0.40	C
SK09	7.688037317	100.38348	0.26	0.90	C
Wat Prao					
SK10	7.690486384	100.37947	0.968	0.60	C
Yang En					
SK11	7.690255309	100.37674	0.746	0.64	C

Aliquots preparation

During the OSL dating procedure, the samples were carefully managed under subdued red-light conditions (640 ± 20 nm). Sample tubes were unsealed, and the outer sections of the samples were utilised to determine the dose rate. Inner portions of the samples, which had remained shielded from light exposure, were utilized for the assessment of equivalent dose (D_e). Two types of grains were employed in the determination of D_e values: The coarse grains, and the fine grains. Initially, sediment samples were sieved to obtain the coarse grains (100 - 200 µm). Subsequently, these coarse grains were subjected to treatment involving a 10 % hydrogen peroxide (H_2O_2) solution to eliminate organic matter and a 10 % hydrochloric acid (HCl) solution to extract carbonates. A sodium-polytungstate solution ($3Na_2\ WO_4\ 9WO_3\ H_2O$) was prepared with 2 varying densities (2.62 and 2.70 $g \cdot cm^{-3}$) to extract the treated grains and obtain a quartz-rich fraction (density: 2.65 $g \cdot cm^{-3}$). After each step, treated samples underwent rinsing with deionized water many times (3 - 5 times) to remove any residual solutions and adjust their density. Subsequently, the samples were left to dry in a desiccator. Subsequently, the quartz-rich fractions were subjected to etching with hydrofluoric acid (HF) for approximately 45 min to eliminate a surface layer, approximately 20 - 25 µm in thickness, which had been influenced by external alpha-irradiation, and to dissolve any remaining feldspar. This was followed by rinsing of the treated quartz-rich fractions in a 10 % hydrochloric acid solution to eradicate fluorides that might have precipitated during this etching process. For the finer grain fraction, ranging from 4 - 11 µm, sediment samples were fractionated using an Atterberg cylinder with a method based on Stoke's law. A solution of ammonia (NH_3) was introduced to create a suspension, and the fine grain fractions were subsequently processed. A solution of sodium oxalate was added, and the samples were left to dry overnight in a desiccator. Finally, both coarse grain and fine grain of the quartz-rich fraction were then mounted into 10 aliquot discs.

Determination of equivalent dose (D_e)

The measurement of the luminescence signal for all samples was conducted using a Lexsyg smart TL/OSL reader that was equipped with a built-in 90Sr/90Y beta source, which provided a consistent dosage rate of 0.060 ± 0.001 $Gy \cdot s^{-1}$. A modified single-aliquot-regenerative dose (SAR) protocol was applied to

determine the equivalent (D_e) dose [15]. Before conducting OSL measurements, every aliquot disc underwent a 40 s exposure to infrared (IR) radiation at a temperature of 125 °C. This step was performed in order to eliminate any IR-sensitive signal and remove any potential feldspar contamination. The quartz samples were subjected to stimulation using green light-emitting diodes (LEDs) generating light at a wavelength of 470 ± 5 nm for a duration of 40 s. The optical stimulated luminescence (OSL) signal was observed using an EMI 9235QB15 photomultiplier tube that was connected to a 7.5 mm Hoya U-340 detection filter.

A minimum of 10 aliquots in each sample were assessed for the purpose of determining and analysing the concentration of D_e. This analysis was conducted using Analyst software v4.56 [28]. The intensity of OSL signal is determined by measuring the signal within the time range of 0 - 0.8 s from the beginning and 20 - 40 s from the end, after subtracting the background. The estimation of dose-response curves can be achieved by the utilisation of an exponential function. The approval of individual D_e value was determined based on the following criteria: (i) The recycling ratio exhibits a value of 1 ± 0.1. (ii) The test dose error is found to be less than 10 %. (iii) The recuperation ratio is less than 10 % of the natural signal. The statistical values of the D_e distribution for well-bleached sediments were obtained and enhanced using 2 models: The central dose model (CDM) [16,29] and the average dose model (ADM) [17]. These models were implemented using the 'Luminescence' package in the R software [30]. The intrinsic overdispersion (σm) of ADM was determined by applying 'CDM' to a dose recovery experiment (SK09) at the preheating temperature of choice; the calculated value is 0.04733. The burial age of the sediment sample is then provided by dividing the equivalent dose (D_e) by the dose rate ($\dot{D}$).

Dose rate and age calculation

The sediment samples from both ends of the opaque stainless-steel tube, exposed to sunlight during sampling were processed under a normal light room. Samples were weighted before and after oven-dried at 50 °C. The water content was then calculated with 5 % uncertainty. After that, the samples were milled to achieve a homogenous grain size. The milled samples approximately 120 g were then stored and sealed air-tight into a plastic container for a month to gain an equilibrium condition of ^{222}Rn - ^{226}Ra. All samples were analyzed by high resolution gamma spectrometry (High Purity Germanium; HPGe). Each sample was measured for 3 days to obtain optimum counts for the required radionuclide peaks. The activity of radioactive elements (^{238}U, ^{232}Th and ^{40}K) were converted to the dose rate using conversion factors [31]. The cosmic ray dose rates were estimated from the geomagnetic latitude, as well as surface altitude and the burial depth of the samples below surface [32]. Subsequently, the dose rates and ages were calculated using online software '*Dose Rate and Age Calculator* or DRAC' [33].

Previous data integration

Numerous studies were conducted in the larger Songkhla lagoon area [11,20-24]. There were 2 dating techniques: ^{14}C and TL dating. All of the radiocarbon ages were reported in the year before present (year BP). However, in geological interpretation, those ages must be calibrated due to the fluctuation of cosmic radionuclides during the Quaternary. The *IntCal* (**R** package for radiocarbon age calibration) was applied; hence, radiocarbon ages here reported in cal year BP can be joined with the TL and OSL ages.

Results and discussion

Fieldwork and geological cross-section

The surface altitudes based on RTK technique were between −0.74 - 2.11 m, while the high-water level was 0.36 m. The possible geologic unit was assumed based on the geological map of Department of Mineral Resources and confirmed by fieldwork. They consisted of 3 sand ridges: ~2 m height at the east-most (100 m from the present coastline), and 1 m height at the middle (400 m from the present coastline) and west-most (1,200 m from the present coastline).

At the most-eastern sand ridge, a 1.40-m-deep trench showed fine sand from 0 - 1.32 and 1.34 - 1.4 m (215.042 μm-mean-grain-size) and 2-cm-thick coarse sand at 1.32 - 1.34 m. Moreover, we observed a yellowish-brown layer in the fine sand layer. This indicates the vegetation that induced the aeolian process. Behind the east-most ridge, there was a shrimp pond, which showed muddy sediments.

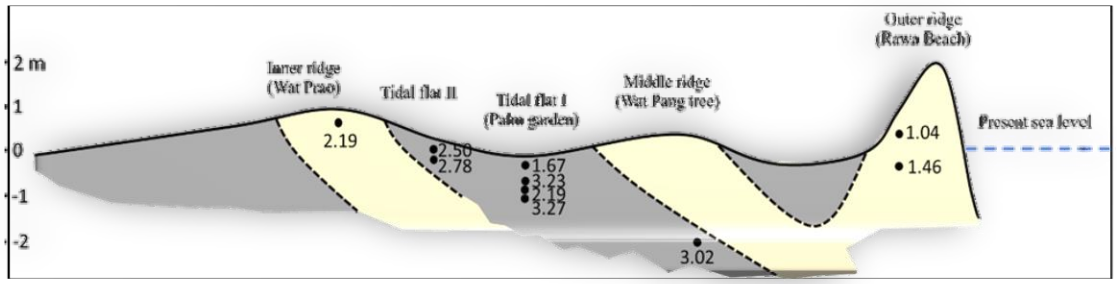

Figure 2 Topographic cross-section (dash line in **Figure 1**) of the study site with geological unit in different colours. Grey = Older tidal flat; Yellow = Older beach ridge; Numbers are OSL age results in ka, (Right side is the present-day coastline).

Grain size analysis and sedimentological description

Outer sand ridge (Rawa beach) 100 m from modern beach

The sediment is mainly composed of fine sand, moderately well sorted from the surface to 1.32 m depth. The grain size distribution is coarse-skewed and very leptokurtic. The topmost 0.15 m is the topsoil layer characterized by dark grey sandy soil. The light yellowish grey fine sand at 0.15 - 0.5 m depth and the sediment colour gradually changes from light yellow to more brownish yellowish with red layer at 0.65, 0.78, 0.83 and 0.93 m and the sediment colour are more greyish with more humid at the depth of 1.00 - 1.32 m. The coarse sand with moderate sorted was found at the depth of 1.32 - 1.40 m and the sediment colour changed to light greyish, with moderate sorted. The grain size distributions are fine-skewed and platykurtic.

Middle sand ridge (Wat Pang tree) 400 m from modern beach

The sediment is mainly composed of very fine sand and moderately sorted. The grain size distribution indicates nearly symmetrical and very leptokurtic. Shell fragments were found in this area.

Tidal flat (I) between the middle and inner sand ridges, 700 m from modern beach

The uppermost layer of sediment, extending to a depth of 0.40 m, exhibits a dark grey clay and changing to a combination with brownish yellow from 0.40 - 0.56 m. The sediment colour then gradually changes to light grey clay with brownish yellow and dark brown dot at a depth of 0.56 - 1.33 m. The mean grain size slightly increases at 1.33 - 1.54 m from clay size to very fine sand with moderately well sorted. The grain size distribution is fine skewed with very platykurtic. Abundance of shell fragments was observed at 1.19 m and between 1.33 - 1.54 m from the surface layer. Below, the grain size decreased to clay size (4 - 11 µm) and a light grey with yellowish brown. Additionally, salt water and shell fragments were indicated during field work and a quantity of mica sheet were identified during laboratory examination.

Tidal flat (II) between the middle and inner sand ridges, 900 m from the modern beach

The topmost layer of sediment (0.90 m) consists of a black topsoil. The underlying layer (0.90 - 0.27 m depth) is composed of silty clay and grey colour. Between a depth of 0.27 - 0.47 m, the sediment was dominated by clay and small sand size with an ocre colour. Unknown stones were found at this layer. At 0.47 m from surface, the groundwater was discovered. Below depth of 0.47 m, the sediment is dominated by sand and shell fragments were found at a depth of 0.70 m from the surface.

Inner sand ridge (Wat Prao), 1,400 m from modern beach

The sediment consists of moderately well sorted and very fine sand. The grain size distribution is fined-skewed and very leptokurtic. No fragment shells or sedimentary structures were identified within this excavation site.

Tidal flat (III), 1,600 m from modern beach

The sediment, the topmost layer (0.90 m) consists of a very dark topsoil. The underlying layer (0.90 - 0.15 m depth) is composed of dark grey sand with shell fragments. At a depth of 0.15 to 0.24 m, the colour of the sediment transforms to yellowish-brown sand. Below that, the grain size diminished to the size of clay and the colour was light grey with a brownish colour. Following 0.54 m, extremely dark grey sand, shell fragments and groundwater were discovered.

Luminescence dating

The dose recovery test for SK09 was performed by adjusting the preheat temperatures within the range of 180 to 260 °C, with increments of 20 °C. Subsequently, the preheating temperature of 240 °C consistently replicated the approved laboratory dosages, therefore it was employed for all D_e measurements conducted in the present study (**Figure 3**).

The OSL decay curve of SK01 (**Figure 4(a)**) was obtained using a known artificial irradiation (1 s dosed = 0.060 ± 0.001 Gy), and the determination of dose response for each aliquot can be performed by applying an exponential function, as illustrated in **Figure 4(b)**. The application of quartz SAR-OSL has proven to be highly effective in accurately determining the age of the coastal sediment samples that were analysed in the present study.

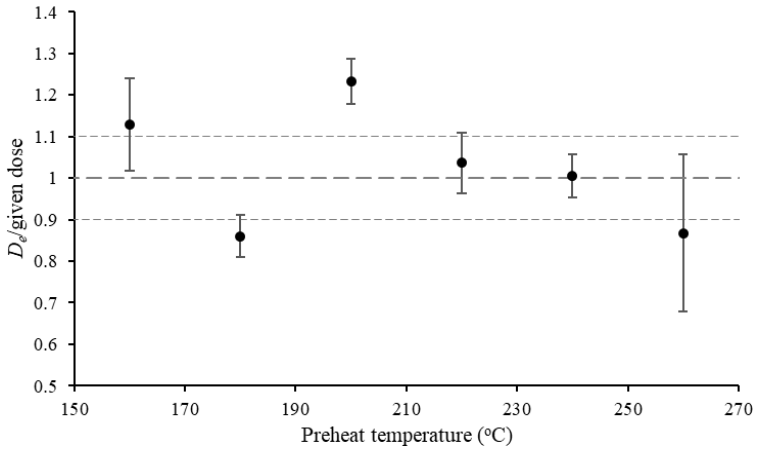

Figure 3 Dose recovery test of SK09 for a preheated temperature of 240 °C.

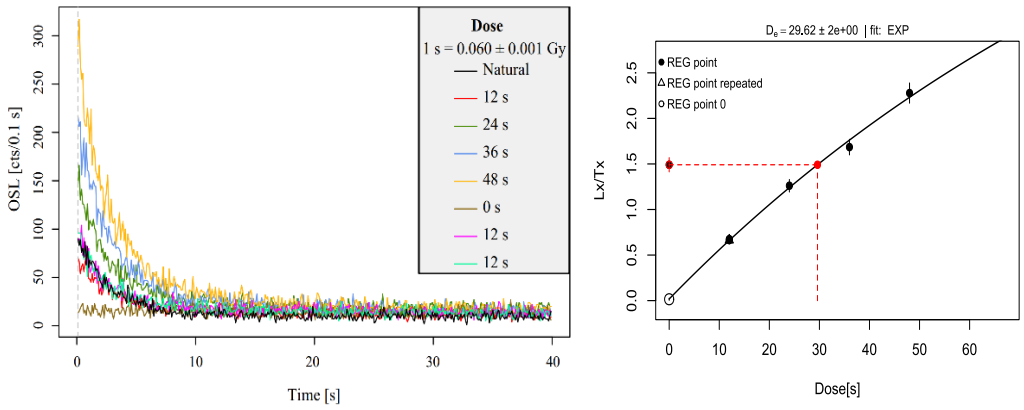

(a) (b)

Figure 4 Example of (a) the OSL decay curve of SK01 and (b) the dose-response curves of SK01.

Dose rate

The effective dose rate ($\dot{D}$) ranged from 1.33 ± 0.05 to 3.97 ± 0.13 Gy·ka^{-1}. The results of the $\dot{D}$ determination is given in **Table 2**. The lowest $\dot{D}$ values obtained from sandy unit of outer sand ridge range from 1.33 ± 0.05 to 1.53 ± 0.07 Gy·ka^{-1}. The highest $\dot{D}$ values observed from clay unit of the tidal flat range from 3.21 ± 0.09 to 3.97 ± 0.13 Gy·ka^{-1}.

Th, U and K are radioactive element-containing minerals. K exhibits a high solubility in water and displays greater mobility in comparison to both Th and U. It can be easily leached from the source and carried to low-lying locations. This leads to a reduced concentration of K in all sedimentary units. Especially with the coarser grain size of sandy units [34]. The released Th during weathering demonstrates a higher capacity for adsorption onto clay minerals [34]. This can be attributed to its lack of solubility and less mobility, resulting in its capacity to persist within its original location. Hence, it was observed that the levels of Th in sediment composed of silty clay and clay were higher compared to those in sandy units.

In addition, shell fragments [35] were used as indicators of the marine environment and mica particles were used as indicators for energy level and depositional environment [36], and they have been used to determine paleoenvironments. The utilisation of mica has been employed in the assessment of energy gradients within depositional settings. Large amounts of mica with fine sediment (SK04-SK07) imply a region of low-energy environments [37], such as lakes, lagoons or floodplains, where there is insufficient energy to transport fine particles. Consequently, fine sediments such as clay and silt tend to accumulate, could be found at palm garden.

Four OSL samples were collected at depths of 0.35, 1.12, 1.40 and 1.60 m at the palm garden site. The OSL ages at 1.40 m (SK06) were younger than those at 1.12 m (SK05), indicating inconsistency between ages and sampling site at 1.12 and 1.40 m, as shown in **Table 2**. Based on the findings of this experiment, it is possible that varying sediment sizes exhibited differential abilities in absorbing distinct quantities of radioactive elements. Clearly, SK06, a sandy unit at the palm garden site, contained higher concentrations of Th, U and K than the sandy unit identified on the former beach at Rawa Beach. It is important to acknowledge that the palm gardens (SK05 and SK06) display a thick layer of clay on top and coarse sand on the bottom. Therefore, the clay sediment above the coarser sand can enter between the coarser sand that was deposited at a lower level over time. Due to the characteristics of clay, radioactive nuclides are typically absorbed more by clay or finer sediments [34]. When clay accumulates or becomes compacted near sand, radioelements Th, U and K may have an impact on coarser sand, resulting in slightly higher radioactivity than coarse sand at Rawa Beach. This layer of sand sediment exhibits elevated and inconsistent radioactivity due to the increased abundance of radionuclides. Consequently, with the expansion of radioelements, there is a corresponding increase in their radiation dose, leading to a significantly younger OSL age estimation in the palm garden at the coarse grain at a depth of 1.40 m.

Table 2 Summary data of OSL dating, including moisture content, concentration of radionuclide elements (U, Th and K), the total dose rate ($\dot{D}$), the number of accepted aliquots (n: Accepted/measured), equivalent dose calculated by the central dose model (CDM) and their final OSL age estimated, and the average dose model (ADM) and their final OSL age estimated.

ID	Moist. (%)	K (%)	Th (ppm)	U (ppm)	$\dot{D}$ (Gy·ka^{-1})	n	Central dose model		Average dose model	
							CDM (Gy)	Age (ka)	ADM (Gy)	Age (ka)
SK01 (80)	2.79	0.94 ± 0.03	3.00 ± 0.23	1.10 ± 0.07	1.53 ± 0.07	10/10	1.58 ± 0.06	1.03 ± 0.06	1.59 ± 0.06	1.04 ± 0.06
SK02 (133)	17.90	0.85 ± 0.03	4.10 ± 0.26	1.26 ± 0.08	1.33 ± 0.05	10/10	1.93 ± 0.09	1.45 ± 0.09	1.94 ± 0.08	1.46 ± 0.09
SK03 (200)	29.45	2.11 ± 0.05	21.85 ± 0.61	4.80 ± 0.15	3.62 ± 0.12	10/10	10.92 ± 0.25	3.02 ± 0.12	10.92 ± 0.20	3.02 ± 0.12
SK04 (35)	33.81	2.20 ± 0.05	26.41 ± 0.63	5.65 ± 0.15	3.97 ± 0.13	10/10	6.62 ± 0.21	1.67 ± 0.08	6.63 ± 0.21	1.67 ± 0.08
SK05 (112)	34.08	2.28 ± 0.05	23.20 ± 0.59	4.35 ± 0.14	3.64 ± 0.12	10/10	11.76 ± 0.22	3.23 ± 0.12	11.75 ± 0.21	3.23 ± 0.12
SK06 (140)	20.96	3.21 ± 0.06	5.84 ± 0.35	1.51 ± 0.09	3.32 ± 0.13	10/10	7.14 ± 0.54	2.15 ± 0.18	7.26 ± 0.57	2.19 ± 0.19
SK07 (160)	54.73	2.19 ± 0.05	25.39 ± 0.64	4.99 ± 0.15	3.21 ± 0.09	10/10	10.30 ± 0.35	3.21 ± 0.14	10.51 ± 0.35	3.27 ± 0.14
SK08 (40)	27.85	2.04 ± 0.05	22.50 ± 0.58	5.39 ± 0.15	3.80 ± 0.13	10/10	9.16 ± 0.83	2.41 ± 0.23	9.51 ± 1.12	2.50 ± 0.31
SK09 (90)	18.33	1.75 ± 0.05	3.98 ± 0.29	0.95 ± 0.07	2.01 ± 0.08	9/10	5.51 ± 0.32	2.75 ± 0.20	5.57 ± 0.34	2.78 ± 0.20
SK10 (60)	18.46	2.30 ± 0.05	4.53 ± 0.30	1.39 ± 0.08	2.59 ± 0.10	10/10	5.47 ± 0.49	2.12 ± 0.21	5.67 ± 0.57	2.19 ± 0.24
SK11 (64)	14.26	1.89 ± 0.05	13.36 ± 0.44	3.22 ± 0.11	3.20 ± 0.12	10/10	0.96 ± 0.22	0.30 ± 0.07	1.23 ± 0.42	0.38 ± 0.13

Distribution of equivalent dose (D_e)

The D_e values obtained from the CDM exhibit a range of 0.96 ± 0.22 to 11.76 ± 0.22 Gy, while most of the D_e values obtained from the ADM range exhibit slightly higher values compared to the CDM, spanning within the range of 1.23 ± 0.42 to 1.75 ± 0.21 Gy (**Table 2**). Generally, the distribution of D_e values exhibited a unimodal distribution curve characterised by a relatively low degree of dispersion. Nevertheless, certain samples exhibited a significantly greater level of dispersion. In the present investigation, the overdispersion values varied between 8 and 70 %.

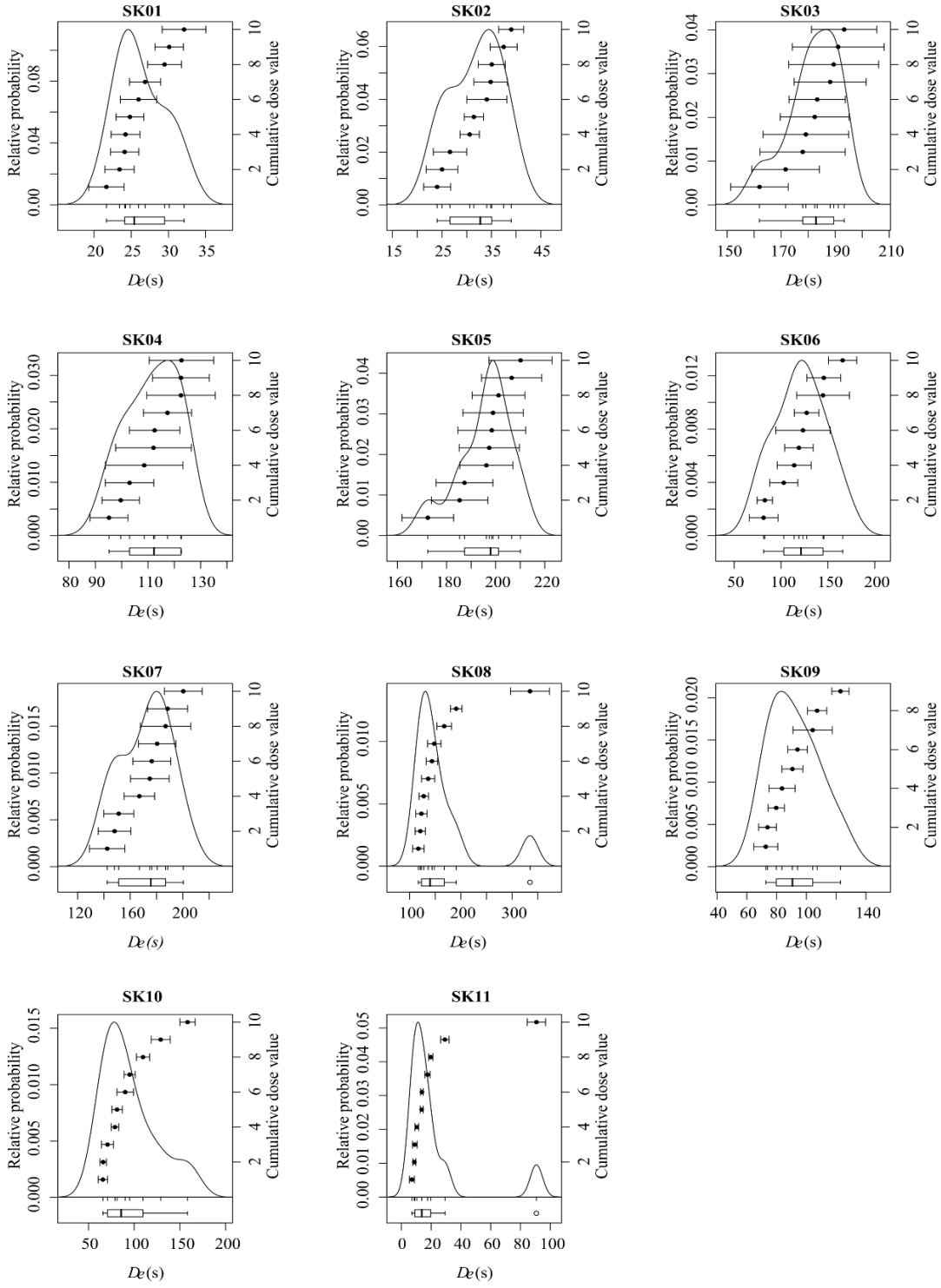

Figure 5 D_e distribution curves represented as kernel density estimate plots for samples SK01 to SK11.

The D_e distributions of SK01, SK02 and SK09 show a relatively low overdispersion (below 20 %) [38,39]. This low overdispersions, along with a narrow D_e distribution, suggests homogeneity, with most grains sharing identical D_e values, implying a complete OSL signal reset during deposition [38-40]. Contrastingly, SK08, SK10 and SK11 samples clearly display significant overdispersion. Specifically, SK08 and SK10 exhibit 27 % overdispersion each, while SK11 stands out with a substantial 70 % overdispersion. Moreover, SK10 shows a slight positive skewness. The narrow D_e distribution range in

SK08 and SK11. However, both of them characterized by higher D_e values, contribute to a notable overdispersion, as depicted in **Figure 5**. The positive skewness observed in the data may have resulted from incomplete bleaching before deposition or potentially due to fluctuations in micro-dosimetry. Likewise, the emergence of an outlier might be attributed to heightened localised radiation or additional external variables affecting the D_e values. For example, the occurrence of zircon in the quartz component, comprising around 5 % of the Songkhla coastal area, can contribute to these phenomena. On the contrary, it is important to acknowledge that there is a low overdispersion and a slight negative skewness. This observation indicates that some aliquots exhibited lower D_e values. This occurrence may be attributed to the existence of more recent sediment particles, potentially resulting from bioturbation, grain re-deposition or post-depositional events [39], as evidenced in the studies conducted by SK02 and SK03.

The analysis of D_e distribution is not possible for SK03, SK04, SK05 and SK07, as they were processed as fine-grain aliquots. Fine-grain aliquots typically comprise approximately 1,000,000 individual grains [38]. Consequently, the limited presence of an adequate number of reset grains may not be apparent due to the mitigating influence of a significant volume of grains. As a result, the application of D_e distribution values has been restricted to larger-sized samples, whereas their use in smaller-sized samples is limited.

Samples from the tidal flat unit in the palm garden were mainly processed as fine-grained aliquots, except for SK06, which was processed as a coarse-grained aliquot. However, despite their varying depths within the unit, the estimated ages for SK06 at a depth of 1.40 m appeared to be younger than those for SK07, which was situated at a depth of 1.12 m, as discussed earlier. This inconsistency in age estimates could potentially be attributed to the differing particle sizes present in the samples. Specifically, SK06 consisted of coarse grains, measuring around 100 - 200 µm, while the fine grain aliquots ranged from approximately 4 to 11 µm. As a result, the saturation characteristics (dose value) tend to decrease as the particle diameter increases [41]. This sediment particle size influences the buried dose and causes it to be underestimated. Nevertheless, the mechanism underlying this particle size dependence on saturation characteristics is not yet completely understood.

In this present study, CDM and ADM were applied to the equivalent dose for age estimation. Both of these age models are highly suitable for materials that underwent complete bleaching. The findings indicate that the estimated ages derived from the CDM in this investigation were somewhat lower compared to the estimated ages obtained from the ADM. The age calculation provided in this study is consistent with previous research on paleosols, suggesting that D_e values generated by the ADM tend to be slightly greater than those obtained from the CDM [42]. Interestingly, comparisons have revealed limitations in CDM, leading to the underestimation of burial doses. Particularly the CDM considers all overdispersion as measurement uncertainty, whereas the ADM distinguishes between intrinsic and other sources of overdispersion. In addition, the CDM calculates the geometric mean rather than the arithmetic mean, which results in an underestimation of age. ADM addresses uncertainties related to the Analyst software version 4.57, such as counting statistics, curve fitting and instrument reliability. These factors affect D_e values and contribute to a significant overdispersion of data [17]. Hence, any variation observed in the age of the ADM-base that is beyond expectations can solely be attributed to extrinsic factors such as micro-dosimetry. Consequently, it has been suggested that applying the ADM to completely bleached materials will reduce any intrinsic uncertainty and increase the age value by providing a more precise and accurate age estimation while also displaying better robustness than the CDM.

Geological interpretation

Only the late Holocene ages were indicated; they range from 0.384 ± 0.132 to 3.016 ± 0.116 ka (**Table 2**). These former beach ridges extended between 100 and 1,600 m from the present-day beach. The estimated age increases with distance from the shoreline as well as with depth below the surface. However, SK11 is relatively contemporary in age, with only 400 years, despite being almost 1.6 km away from the present-day beach. Similarly, the estimated age of SK06 did not correspond with their depth of sampling location, as described earlier. Consequently, it will not be subject to interpretation.

For the inner sand ridges (westernmost), the oldest age of 2.2 ka was found at the site SK10, whereas the youngest age of 0.38 ka was identified at 1.5 km away from the outer sand ridge. The oldest deposit of this beach ridges system yields an age of 3.3 ka and was found at low lying areas which indicate as tidal flat between the inner and outer ridges.

The resulting OSL sample, collected at a distance of 100 m from the present-day Rawa beach, clearly demonstrates the demarcation between the foreshore zone (FS) and the backshore zone (BS). The upper part of this profile consists predominantly of finely grained, massive sand that exhibits moderately well sorted. The presence of stratification was seen within the bottom section of the aeolian sand unit,

characterised by thin layers that exhibited a near-horizontal orientation. The colouring of these layers transitioned gradually from a light-yellow shade to a brownish-yellow shade, with the occurrence of a red layer at a depth of 0.9 m below the surface, which can be attributed to heightened oxidation processes. The previous upper profile has been classified as the backshore (BS). At a depth of 1.32 - 1.44 m below the surface, the lower section of the profile has a layer of coarse-grained sand that displays a moderately sorted. The detected sediment, characterised by its coarse grain size, has been classified as an upper foreshore (FS) deposit. This classification suggests that the sediment was formed in a high-energy environment along the shoreline, estimated to have occurred around 1.46 ka ago. The topmost aeolian unit exhibits evidence of sand accretion in the backshore approximately 1.04 ka ago, suggesting that this previous beach area remained relatively stable for a minimum duration of 400 years.

Beach ridges have previously been used in the context of reconstructing sea levels, as they form through an interaction of fair-weather wave and storm-wave processes, as well as wind activity, thereby providing valuable insights into past environmental conditions. This study focuses on a specific past reconstruction of sea levels. Subsequently, the investigation employed the indicative meaning calculator [9]. The upper limit of sea level indicators of the beach ridge was identified using the modern measured heights of storm wave swash height (SWSH) at 1.8 m amsl, while the lower limit was determined using the modern measured heights of the ordinary berm (Ob) at 0.36 m amsl. Elevation measurements in the estimated Paleo-RSL were derived from the surface altitude and depth obtained at the boundary between the FS and BS. Findings of this study suggest that the initiation of the eastern outer beach ridge occurred approximately 1.5 ka ago, during a period when the sea level was 1.4 m lower than the present msl. Nevertheless, the paleo-sea level observed in this study differed from the findings of a prior study, which indicated that the current sea level had previously reached approximately 1.5 BP [43]. It is important to acknowledge that the data presented here relates primarily to local sea level fluctuations in the past. Additionally, previous geochronological studies relied solely on shell fragments or other organic materials and did not involve the calibration of the ^{14}C age-based findings. Furthermore, it is important to consider the potential effects of vertical tectonic movements in neighbouring regions on this area. This study provides more insight into the influence of vertical land motion, including tectonic uplift and subsidence, on variations in relative sea level (RSL) in peninsular Malaysia. The KUAL station located in Kuala Terengganu provides evidence of vertical land uplift occurring at a rate of 1.18 ± 0.32 m/ka until the year 2005, specifically before the occurrence of the Sumatra-Andaman megathrust earthquakes. In contrast, subsequent vertical land subsidence was seen to be within the range of 0.5 ± 0.12 m/ka. In addition, the data obtained from the GET1 and GET2 stations indicates the need to take into account human subsidence factors, such as sediment compaction and groundwater extraction [44]. This available evidence indicates that both tectonic and human-driven processes have exerted influence on Peninsula Malaysia. This peninsula encompasses the coastal region of Songkhla, which is geographically located inside its boundaries.

Between around 6.9 and 4.5 ka ago, the coastal region of Songkhla underwent a period of increasing sea levels, resulting in the elevation of the sea level to 3 - 4.5 m amsl [1]. Additionally, the geophysical model conducted provided evidence of a highstand of sea level during the mid-Holocene period, specifically at 5 m amsl around 6.0 ka ago, followed by a progressive decline to the present day [45]. Consequently, this area was submerged in a shallow marine environment. From 3.7 to 2.7 ka ago, the sea level declined [43]. This period signifies the early stages of the formation of the beach ridge system that is currently being studied. Indeed, by conducting an accurate examination of the sediment composition and employing age determination by OSL dating techniques, significant knowledge can be obtained regarding the chronological sequence of deposition for both the runnel and the old beach, significant information can be obtained regarding the chronological sequence of deposition for both the runnel and the old beach. The sediment found in this particular location is predominantly composed of reasonably well-sorted, very fine sand that underwent deposition around 3.27 ka ago (palm garden). Similarly, the moderately sorted, very fine sand collected from a depth of 2 m below the surface, originating from beneath the massive sand at the Wat Pang tree trench, displayed a deposition time around 3.02 ka ago. This evidence indicates that the sand ridge and adjacent plain behind it were formed simultaneously. Significantly, both regions exhibited considerable amounts of shell fragments. The beach ridge system under investigation is believed to have assumed the form of a submerged longshore bar (Wat Pang Tree), along with a longshore trough (palm garden). It is hypothesised that these landforms underwent parallel extension in relation to the prevailing coastlines throughout the period of stable sea levels in the Holocene epoch [46]. As the elevation of the longshore bar increased, a corresponding depth of the longshore trough occurred, resulting in the development of a low-energy environment that contributed to the accumulation of smaller particles. As the progressive decline in sea levels occurred, the longshore bar eventually reached a state of equilibrium with

the sea level, resulting in its transformation into the newly formed beach. Following this, the previous beach became isolated, and the longshore trough located behind the longshore bar developed into a new lagoon. Between 2.19 - 1.46 ka ago (**Table 2**), the prevailing dry climate and intense winds may have caused the redistribution of wind-blown sand onto the pre-existing sandy beaches as well as the newly created beach resulting from wave action.

Insufficient data in the present study prevents the determination of any potential connection between the formation of beach ridges and the underlying processes involved, specifically in relation to the combination of longshore bars. The occurrence of beach ridges, which arise from the merging of longshore bars, is rather uncommon due to the requirement of appropriate environmental circumstances [2]. These conditions usually appear in regions marked by a gradual incline of the shoreline and a limited range of tidal fluctuations, necessitating the influx of sediment from the adjacent nearshore area [46] and the absence of long-period swell [47]. Despite the apparent microtidal conditions prevalent in our region, which are marked by tidal changes of less than 1 m [48], there remains a significant lack of exploration about the beach ridge, specifically the one formed through the merging of longshore bars. The Mekong River delta is the nearest point of interest [49].

Previous research conducted in this particular field [11,22] investigated 2 specific boreholes, STwat and STMH, located in the middle part of the main former beach ridge. STwat is located in the south (Zone 47, 0659123 E 0826160 N). STMH, on the other hand, is located in the north (Zone 47, 0658568 E 0827566 N). These boreholes underwent ^{14}C and TL dating techniques. In spite of this, all ^{14}C ages were reported in years before the present (BP). To increase the accuracy and reliability of estimated ages derived from ^{14}C, the *intCal* package of the R software must be used to calibrate them. Consequently, ^{14}C dates were represented in calibrated years before the present (cal. BP).

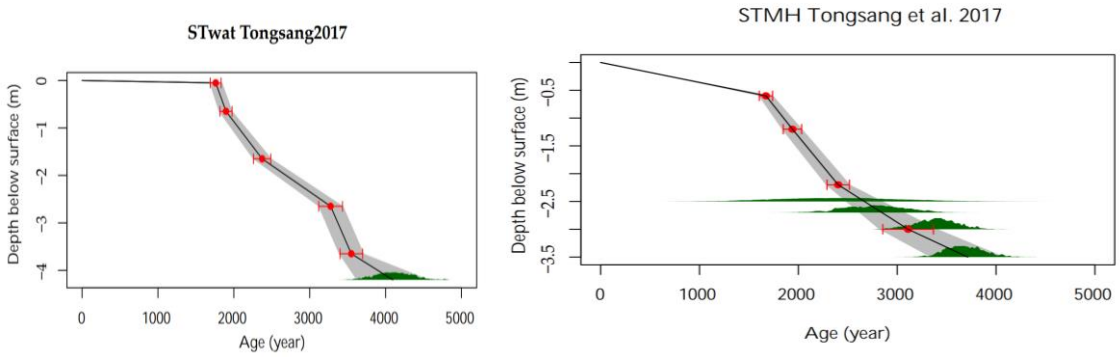

Figure 6 Bayesian age-depth model [50] of TL and ^{14}C dating from STwat and STMH borehole [22].

The STwat borehole data reveals the following TL ages at different depths below surface area: 0.05, 0.65, 1.65, 2.65 and 3.65 m. These depths have corresponding dates of 1.761 ± 0.06, 1.897 ± 0.08, 2.373 ± 0.11, 3.275 ± 0.16 and 3.548 ± 0.15 ka, respectively. The ^{14}C dating estimated the age at a depth of 4.2 m to be 4,096 ± 479 cal. BP. While The TL ages of the STMH boreholes at depths of 0.6, 1.2, 2.2, and 3 m below surface area are calculated to be 1.672 ± 0.06, 1.940 ± 0.09, 2.403 ± 0.11 and 3.110 ± 0.26 ka, respectively. Furthermore, the presence of ^{14}C in this pit indicates the ages at various depths below surface area. These depths include 2.5, 2.7, 3 and 3.5 m with corresponding ages of 2,453 ± 1,189, 2,835 ± 542, 3,371 ± 406 and 3,713 ± 377 cal. BP.

Based on the geological map, it can be shown that the accumulation of sediment originated in a southward direction (STwat) and extended towards the north (STMH). Consequently, an investigation was conducted in order to confirm the hypothesis by examining the characteristics of soil formation in each borehole. Evidence of soil development was observed within the whole depth of the STwat borehole, at a depth ranging from 1.2 - 1.9 m below surface area. This soil development is described by a brownish-yellowish brown colour, with a reddish spot situated below a black sediment layer. The age of the sediment, as determined using TL dating, was found to be 2.373 ka ago. Likewise, STMH has an accumulated layer thickness of 3.5 m. The sediment consisted of white sand covered by a rust-coloured brownish sand. This layer formed approximately 1.940 ka ago at a depth of 0.3 - 1.4 m below surface area. Compared to the 2 previously mentioned works, this present investigation at Rawa Beach (SK01 and SK02), is located at the northernmost point. The sediment gradually changed from pale yellow to brownish-yellow at a depth of 0.65 - 0.95 m below the surface, with red layers at 0.65, 0.78, 0.83 and 0.93 m. According to the OSL age,

soil formation in the region occurred approximately 1.04 ka ago. From the depth and age data, it can be concluded that the deposits originated from STwat, STMH and Rawa Beach, respectively. The progradation of the sand ridges in our study was agreed with the explanation by [20,21].

Conclusions

The findings of the present investigation, which include 11 geochronological data sets and 5 sedimentology studies, provide evidence of a late-Holocene regression in the Sathingpra peninsula. Two aliquot types, coarse- and fine-grained quartz, have been applied to the modified SAR technique to indicate the process of age estimation. The present study introduced the initial success of accurate quartz dating using fine-grained quartz. In general, the OSL dating reveals a late Holocene regression in the Sathingpra peninsular. OSL ages of the swale (or lagoon) and the middle beach ridge suggests that there was a period of stable sea level throughout the late Holocene, approximately 3.3 to 1.7 ka ago.

After this stable period, a sea level regression occurred parallel with an increased aeolian activity, resulting in the formation of shore-parallel sand ridges approximately 1.5 ka ago. During this period, the sea level was recorded to be 1.4 m lower than the present msl, resulting in a transition of the lagoon into a tidal flat. Other research related stratigraphy and radiocarbon dating provided evidence for a northwards development of the middle beach ridge. However, for the sea level reconstruction it is crucial to carefully consider also possible influences by tectonic uplift/subsidence and human activities (adding/removing sand) contributing the overall shoreline development. Finally, interdisciplinary research is essential to enhance the accuracy of reconstructing sea level fluctuations and environmental changes, here in the Songkhla coastal region and elsewhere.

Acknowledgments

We would like to extend our gratitude to Kittiwara Sornplang and Mila Geindre (ENSTRA Bretagne Engineering School, Brest, France) for their assistance with the field work. This research was supported by Prince of Songkla University, Thailand, with the grant number ENV6402075S and the Coastal Oceanography and Climate Change Center (COCC).

References

[1] P Noppradit, C Schmidt, H Dürrast and L Zöller. Late quaternary evolution of Songhkla coast, Southern Thailand, revealed by OSL dating. *Chiang Mai J. Sci.* 2019; **46**, 152-64.

[2] T Tamura. Beach ridges and prograded beach deposits as palaeoenvironment records. *Earth Sci. Rev.* 2012; **114**, 279-97.

[3] T Tamura, Y Saito, MD Bateman, VL Nguyen, TKO Ta and D Matsumoto. Luminescence dating of beach ridges for characterizing multi-decadal to centennial deltaic shoreline changes during Late Holocene, Mekong River delta. *Mar. Geol.* 2012; **326-328**, 140-53.

[4] EG Otvos. Beach ridges - definitions and significance. *Geomorphology* 2000; **32**, 83-108.

[5] L Alappat, M Frechen, SS Kumar, DSS Babu, R Ravur and S Tsukamoto. Evidence of Late Holocene shoreline progradation in the coast of Kerala, South India obtained from OSL dating of palaeo-beach ridges. *Geomorphology* 2015; **245**, 73-86.

[6] S Kongsen, S Phantuwongraj and M Choowong. Distinguishing Late Holocene storm deposit from shore-normal beach sediments from the Gulf of Thailand. *Front. Earth Sci.* 2021; **9**, 625926.

[7] D Brill, N Klasen, H Brückner, K Jankaew, A Scheffers, D Kelletat and S Scheffers. OSL dating of tsunami deposits from Phra Thong Island, Thailand. *Quaternary Geochronology* 2012; **10**, 224-9.

[8] D Brill, N Klasen, K Jankaew, H Brückner, D Kelletat, A Scheffers and S Scheffers. Local inundation distances and regional tsunami recurrence in the Indian Ocean inferred from luminescence dating of sandy deposits in Thailand. *Nat. Hazards Earth Syst. Sci.* 2012; **12**, 2177-92.

[9] T Lorscheid and A Rovere. The indicative meaning calculator - quantification of paleo sea-level relationships by using global wave and tide datasets. *Open Geospatial Data Software Stand.* 2019; **4**, 10.

[10] P Surakiatchai, M Choowong, P Charusiri, T Charoentitirat, S Chawchai, S Pailoplee, A Chabangborn, S Phantuwongraj, V Chutakositkanon and S Kongsen. Paleogeographic reconstruction and history of the sea level change at Sam Roi Yot National Park, Gulf of Thailand. *Trop. Nat. Hist.* 2018; **18**, 112-34.

[11] B Tongsan. 2017, Dating of Sating-Pra peninsular in southern Thailand by radiocarbon and thermoluminescence techniques. Ph. D. Dissertation. Thaksin University, Songkhla, Thailand.

[12] P Nimnate, V Chutakositkanon, M Choowong, S Pailoplee and S Phantuwongraj. Evidence of Holocene sea level regression from Chumphon coast of the Gulf of Thailand. *ScienceAsia* 2015; **41**, 55-63.
[13] M Kilian, B Van Geel and JVD Plicht. ^{14}C AMS wiggle matching of raised bog deposits and models of peat accumulation. *Quaternary Sci. Rev.* 2000; **19**, 1011-33.
[14] F Preusser, D Degering, M Fuchs, A Hilgers, A Kadereit, N Klasen, M Krbetschek, D Richter and JQ Spencer. Luminescence dating: Basics, methods and applications. *Eiszeitalter Gegenwart Quaternary Sci. J.* 2008; **57**, 95-149.
[15] AS Murray and AG Wintle. Luminescence dating of quartz using an improved single-aliquot regenerative-dose protocol. *Radiat. Meas.* 2000; **32**, 57-73.
[16] RF Galbraith and RG Roberts. Statistical aspects of equivalent dose and error calculation and display in OSL dating: An overview and some recommendations. *Quaternary Geochronology* 2012; **11**, 1-27.
[17] G Guérin, C Christophe, A Philippe, AS Murray, KJ Thomsen, C Tribolo, P Urbanová, M Jain, P Guibert and N Mercier. Absorbed dose, equivalent dose, measured dose rates, and implications for OSL age estimates: Introducing the average dose model. *Quaternary Geochronology* 2017; **41**, 163-73.
[18] Department of Mineral Resources. *Geological map of Changwat Songkhla*. Department of Mineral Resources, Songkhla, 2007.
[19] Department of Mineral Resources. *Geological map of Changwat Songkhla. Scale 1*. Department of Mineral Resources, Songkhla, 2014.
[20] N Chaimanee. 1989, Geological mapping of the holocene deposits in the coastal plain of Ban Sanamchai Area, Southern Thailand. Master Thesis. Free University of Brussels, Brussels, Belgium.
[21] N Chaimanee and S Tiyapirach. On the coastal morphology of Songkla province, southern Thailand. *In*: Proceedings of the 1st symposium on Geomorphology and Quaternary of Thailand, Bangkok, Thailand. 1983.
[22] B Tongsang, N Chusiri, P Kessaratikoon and T Putsukee. Paleogeography of Sating-Pra Peninsula, southern Thailand. *J. Yala Rajabhat Univ.* 2019; **14**, 73-84.
[23] B Tongsang. Evidence of Paleo sea level change in Middle Holocene, lower part of Sating-Pra peninsula region, southern Thailand. *YRU J. Sci. Tech.* 2021; **6**, 181-9.
[24] B Tongsang, M Daoh, J Hemsalammad and W Meeped. Age of Sa-ting Pra peninsula, Songkhla Province from ^{14}C dating of shells. *Thaksin Univ. J.* 2011; **14**, 146-50.
[25] TG Farr, PA Rosen, E Caro, R Crippen, R Duren, S Hensley, M Kobrick, M Paller, E Rodriguez, L Roth, D Seal, S Shaffer, J Shimada, J Umland, M Werner, M Oskin, D Burbank and D Alsdorf. The shuttle radar topography mission. *Rev. Geophys.* 2007; **45**, RG004.
[26] MJ Aitken. *Thermoluminescence dating*. Academic Press, Massachusetts, 1985.
[27] RL Folk and WC Ward. Brazos river bar (Texas); a study in the significance of grain size parameters. *J. Sediment. Res.* 1957; **27**, 3-26.
[28] GAT Duller. The analyst software package for luminescence data: Overview and recent improvements. *Ancient TL* 2005; **33**, 35-42.
[29] S Kreutzer, C Schmidt, MC Fuchs, M Dietze, M Fischer and M Fuchs. Introducing an R package for luminescence dating analysis. *Ancient TL* 2012; **30**, 1-8.
[30] R Core Team. *R: A language and environment for statistical computing.* R Foundation for Statistical Computing, Vienna, Austria, 2020.\
[31] G Guérin, N Mercier and G Adamiec. Dose-rate conversion factors: Update. *Ancient TL* 2011; **29**, 5-8.
[32] JR Prescott and JT Hutton. Cosmic ray contributions to dose rates for luminescence and ESR dating large depths and long-term time variations. *Radiat. Meas.* 1994; **23**, 497-500.
[33] JA Durcan, GE King and GAT Duller. DRAC: Dose rate and age calculator for trapped charge dating. *Quaternary Geochronology* 2015; **28**, 54-61.
[34] C Carvalho, R Anjos, R Veiga and K Macario. Application of radiometric analysis in the study of provenance and transport processes of Brazilian coastal sediments. *J. Environ. Radioact.* 2011; **102**, 185-92.
[35] FHR Bezerra, C Vita-Finzi and FP Lima-Filho. The use of marine shells for radiocarbon dating of coastal deposits. *Revista Brasileira Geociências* 2000; **30**, 211-3.
[36] OS Adegoke and DJ Stanley. Mica and shell as indicators of energy level and depositional regime on the Nigerian Shelf. *Mar. Geol.* 1972; **13**, M61-M66.
[37] N Rasul and A Basaham. Mica in the Indus River: An indicator of changes in the depositional environment. *J. King Abdulaziz Univ. Mar. Sci.* 2002; **13**, 77-91.

[38] GA Duller. Single-grain optical dating of quaternary sediments: Why aliquot size matters in luminescence dating. *Boreas Int. J. Quaternary Res.* 2008; **37**, 589-612.
[39] GI López, BN Goodman-Tchernov and N Porat. OSL over-dispersion: A pilot study for the characterisation of extreme events in the shallow marine realm. *Sediment. Geol.* 2018; **378**, 35-51.
[40] A Kunz, D Pflanz, T Weniger, B Urban, F Krüger and YG Chen. Optically stimulated luminescence dating of young fluvial deposits of the Middle Elbe River Flood Plains using different age models. *Geochronometria* 2014; **41**, 36-56.
[41] A Timar-Gabor, JP Buylaert, B Guralnik, O Trandafir-Antohi, D Constantin, V Anechitei-Deacu, M Jain, AS Murray, N Porat, Q Hao and AG Wintle. On the importance of grain size in luminescence dating using quartz. *Radiat. Meas.* 2017; **106**, 464-71.
[42] J Puyrigaud, P Bertran, B Lebrun, C Lahaye, G Guerin and N Limondin-Ozouet. Last interglacial - glacial sequence of palaeosols and calcareous slope deposits at Verteuil (Charente, southwest France). *J. Quaternary Sci.* 2023; **38**, 1321-36.
[43] S Sinsakul. Evidence of quarternary sea level changes in the coastal areas of Thailand: A review. *J. Southeast Asian Earth Sci*. 1992; **7**, 23-37.
[44] W Simons, M Naeije, Z Ghazali, WD Rahman, S Cob, M Kadir, A Mustafar, AH Din, J Efendi and P Noppradit. Relative sea level trends for the coastal areas of peninsular and east Malaysia based on remote and in situ observations. *Rem. Sens.* 2013; **15**, 1113.
[45] BP Horton, PL Gibbard, G Mine, R Morley, C Purintavaragul and JM Stargardt. Holocene sea levels and palaeoenvironments, Malay-Thai Peninsula, Southeast Asia. *Holocene* 2005; **15**, 1199-213.
[46] JR Curray and DG Moore. Holocene regressive littoral sand, Costa de Nayarit, Mexico. *Dev. Sedimentology* 1964; **1**, 76-82.
[47] J Guillén and A Palanques. Longshore bar and trough systems in a microtidal, storm-wave dominated coast: The Ebro Delta (Northwestern Mediterranean). *Mar. Geol.* 1993; **115**, 239-52.
[48] K Aungsakul, M Jaroensutasinee and K Jaroensutasinee. Numerical study of principal tidal constituents in the Gulf of Thailand and the Andaman Sea. *Walailak J. Sci. Tech.* 2007; **4**, 95-109.
[49] T Tamura, K Horaguchi, Y Saito, VL Nguyen, M Tateishi, TKO Ta, F Nanayama and K Watanabe. Monsoon-influenced variations in morphology and sediment of a mesotidal beach on the Mekong River delta coast. *Geomorphology* 2010; **116**, 11-23.
[50] C Zeeden, M Dietze and S Kreutzer. Discriminating luminescence age uncertainty composition for a robust Bayesian modelling. *Quaternary Geochronology* 2018; **43**, 30-9.